

Robust Non-Linear Feedback Coding via Power-Constrained Deep Learning

Junghoon Kim¹ Taejoon Kim² David Love¹ Christopher Brinton¹

Abstract

The design of codes for feedback-enabled communications has been a long-standing open problem. Recent research on non-linear, deep learning-based coding schemes have demonstrated significant improvements in communication reliability over linear codes, but are still vulnerable to the presence of forward and feedback noise over the channel. In this paper, we develop a new family of non-linear feedback codes that greatly enhance robustness to channel noise. Our autoencoder-based architecture is designed to learn codes based on consecutive blocks of bits, which obtains de-noising advantages over bit-by-bit processing to help overcome the physical separation between the encoder and decoder over a noisy channel. Moreover, we develop a power control layer at the encoder to explicitly incorporate hardware constraints into the learning optimization, and prove that the resulting average power constraint is satisfied asymptotically. Numerical experiments demonstrate that our scheme outperforms state-of-the-art feedback codes by wide margins over practical forward and feedback noise regimes, and provide information-theoretic insights on the behavior of our non-linear codes. Moreover, we observe that, in a long blocklength regime, canonical error correction codes are still preferable to feedback codes when the feedback noise becomes high. Our code is available at <https://anonymous.4open.science/r/RCode1>.

1. Introduction

The design of codes has been an important field of research both in information theory and communications, targeting efficient and reliable data transmission across a noisy chan-

nel. We now have near-optimal codes for the canonical open-loop additive white Gaussian noise (AWGN) channel setting first proposed by Shannon (Shannon, 1948), thanks to the extraordinary advancements in code design over a number of decades. However, the design of practical codes for a variety of other important channel models has remained long-standing open problems. In particular, when *feedback* is available in communication systems, i.e., when a transmitter can obtain information on the receive signals through a reverse link from a receiver, it has been shown that while capacity cannot be increased (Shannon, 1956), communication reliability can be improved by utilizing *feedback codes* (Schalkwijk & Kailath, 1966; Butman, 1969; Shayevitz & Feder, 2011; Ben-Yishai & Shayevitz, 2017). However, the design of feedback codes is non-trivial since both the bit stream and feedback information (i.e., past receive signals) should be incorporated into the design. Though feedback codes hold the potential to revolutionize future communication systems, major innovations are needed in their design and implementation.

1.1. Linear Feedback Coding

Over several decades, research on the design of feedback codes for closed-loop AWGN channels mostly focused on the *linear* family of codes, which simplifies code design. The seminal work (Schalkwijk & Kailath, 1966) introduced a linear coding technique for AWGN channels with noiseless feedback, known as the SK scheme, which achieves doubly exponential decay in the probability of error. However, for noisy feedback, the SK scheme does not perform well. In response, (Chance & Love, 2011) introduced a linear coding scheme for AWGN channels with noisy feedback, known as the CL scheme. The CL scheme was further examined and found to be optimal within the linear family of codes under the noisy feedback scenario (Agrawal et al., 2011). There have been attempts to view the linear feedback code design as feedback stabilization in control theory (Elia, 2004) and dynamic programming (Mishra et al., 2021). However, the linear assumption made in these works severely limits their ability to produce optimal codes.

¹Electrical and Computer Engineering, Purdue University, West Lafayette, IN, USA ²Electrical Engineering and Computer Science, University of Kansas, Lawrence, KS, USA. Correspondence to: Junghoon Kim <kim3220@purdue.edu>.

1.2. Deep Learning-Based Channel Coding

A recent trend of research has been examining code design from a deep learning perspective to take advantage of its non-linear structure. Neural encoders and decoders have been shown to improve communication reliability and/or efficiency for various canonical channel settings including open-loop AWGN channels (Nachmani et al., 2016; O’shea & Hoydis, 2017; Dörner et al., 2017; Kim et al., 2018b; Jiang et al., 2019; Habib et al., 2020; Makkuva et al., 2021; Chen & Ye, 2021). In the closed-loop AWGN channel case, Deepcode (Kim et al., 2018a) proposes an autoencoder architecture to generate non-linear feedback codes. Deepcode was shown to outperform SK and CL in terms of error performance across many noise scenarios due to the wider degree of flexibility that non-linearity provides for the creation of feedback codes. Fully-connected neural networks and self-attention modules have also shown significant performance improvements (Ozfatura et al., 2022).

Nevertheless, the vulnerability of these feedback codes to high forward/feedback noise remains understudied. High noise settings have become more pervasive as wireless networks have become denser, making reliable communications even more dependent on channel feedback (Shafi et al., 2017). As pointed out in existing works (O’shea & Hoydis, 2017; Dörner et al., 2017; Jiang et al., 2019), end-to-end learning for the design of codes over point-to-point channels benefits significantly from an autoencoder architecture’s ability to jointly train the encoder and decoder. In this respect, high noise regimes pose two central challenges:

(1) Encoder-decoder mismatch. The encoder (as a transmitter) and decoder (as a receiver) are implemented on two separate platforms. Channel noise therefore causes mismatches in the latent space for coding between encoder and decoder which cannot be directly calibrated due to the limited bandwidth of the forward and feedback links. In Deepcode (Kim et al., 2018a), the encoding structure consists of two distinct phases and operates bit-by-bit, which limits the size of the latent space available to build resilience against high noise conditions. In this work, we consider finite-length bit streams as the units for autoencoder learning to maximally benefit from *noise averaging* that forms the basis for error correction codes (Clark Jr & Cain, 2013), and show the robustness of our codes to high noise levels.

(2) Inefficient power allocation. The transmitter has intrinsic hardware limitations which constrain the encoding outputs in terms of power across channel uses. Coding schemes for point-to-point channels without feedback (O’shea & Hoydis, 2017; Dörner et al., 2017; Jiang et al., 2019) exploit normalization at the encoding outputs to satisfy the power constraint. For power allocation in feedback-enabled channels, Deepcode (Kim et al., 2018a) employs two layers of power weights in addition to a normalization layer. How-

ever, none of these approaches account for the impact of channel noise on the efficacy of power allocation. In this work, we show how power control can be explicitly incorporated into the encoder optimization procedure to obtain constraint satisfaction guarantees.

1.3. Summary of Contributions

- We develop a recurrent neural network (RNN) autoencoder-based architecture for power-constrained, feedback-enabled communications. Using this architecture, we suggest a new class of non-linear feedback codes that build robustness to forward and feedback noise in AWGN channels with feedback.
- Our learning architecture addresses the challenge of encoder-decoder separation over noisy channels by considering the entire bit stream as a single unit to potentially benefit from noise averaging, analogously to error correction codes. We also adopt a bi-directional attention-based decoding architecture to fully exploit correlations among noisy receive signals.
- We augment our encoder architecture with a power control layer, which we prove satisfies power constraints asymptotically. We also provide information-theoretic insights on the power distribution obtained from our non-linear feedback codes, showing that power allocation is highest for early channel uses and then tapers off over time, similar to optimal linear codes.
- Through numerical experiments, we show that our methodology can outperform state-of-the-art feedback coding schemes by wide margins. While other feedback codes are vulnerable to high feedback noise, our codes still perform well as long as the forward noise is reasonable. Also, unlike existing codes, our methodology draws significant benefit from reductions in feedback noise even when the forward noise is high.
- Our results also reveal that there is a high threshold of feedback noise above which canonical error correction codes are still preferable to feedback codes in a long blocklength regime.

2. System Model and Optimization

2.1. Transmission Model

We consider a canonical point-to-point AWGN communication channel with noisy feedback as shown in Figure 1. We assume that the transmission occurs over N channel uses (timesteps). Let $k \in \{1, \dots, N\}$ denote the index of channel use and $x[k] \in \mathbb{R}$ represent the transmit signal at time k . At time k , the receiver receives the signal

$$y[k] = x[k] + n_1[k] \in \mathbb{R}, \quad k = 1, \dots, N, \quad (1)$$

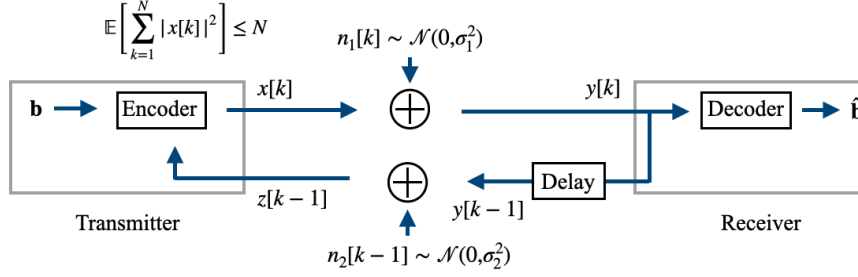


Figure 1. A point-to-point AWGN communication channel with noisy feedback.

where $n_1[k] \sim \mathcal{N}(0, \sigma_1^2)$ is Gaussian noise for the forward channel. We consider an average power constraint as

$$\mathbb{E} \left[\sum_{k=1}^N |x[k]|^2 \right] \leq N. \quad (2)$$

At each time k , the receiver feeds back its receive signal $y[k]$ to the transmitter over a noisy feedback channel, as shown in Figure 1. The transmitter then receives

$$z[k] = y[k] + n_2[k], \quad k = 1, \dots, N, \quad (3)$$

where $n_2[k] \sim \mathcal{N}(0, \sigma_2^2)$ is the feedback noise.

2.2. Functional Form of Encoding and Decoding

The goal of the transmission is to successfully deliver a bit stream $\mathbf{b} \in \{0, 1\}^K$ from the transmitter to the receiver over a noisy channel, where K is the number of source bits. For efficient communication of \mathbf{b} , we consider the following transmitter encoding and receiver decoding procedures.

Encoding. The transmitter encodes the bit stream $\mathbf{b} \in \{0, 1\}^K$ to generate the transmit signals of N channel uses, i.e., $\{x[k]\}_{k=1}^N$. The coding rate is defined by $r = K/N$. Provided feedback from the receiver, the encoding at the transmitter is described as a function of the bit stream \mathbf{b} and the feedback signals $\{z[j]\}_{j=1}^{k-1}$ in (3). Defining an encoding function at time k as $f_k : \mathbb{R}^{K+k-1} \rightarrow \mathbb{R}$, we represent the encoding at time k as

$$x[k] = f_k(\mathbf{b}, z[1], \dots, z[k-1]), \quad k = 1, \dots, N. \quad (4)$$

Decoding. Once the N transmissions are completed, the receiver decodes the receive signals of N channel uses, i.e., $\{y[k]\}_{k=1}^N$ in (1), to obtain an estimate of the bit stream, $\hat{\mathbf{b}} \in \{0, 1\}^K$. Define a decoding function as $g : \mathbb{R}^N \rightarrow \{0, 1\}^K$. Then, we represent the decoding process conducted by the receiver as

$$\hat{\mathbf{b}} = g(y[1], \dots, y[N]). \quad (5)$$

2.3. Optimization for Encoder and Decoder

Block error rate (BLER), the ratio of the number of incorrect bit streams to the total number of bit streams, is commonly

used as a performance metric to assess the communication reliability of bit stream transmissions. Formally, with BLER defined as $\Pr[\mathbf{b} \neq \hat{\mathbf{b}}]$, we consider our encoder-decoder design objective to be the following optimization problem:

$$\underset{f_1, \dots, f_N, g}{\text{minimize}} \quad \Pr[\mathbf{b} \neq \hat{\mathbf{b}}] \quad (6)$$

$$\text{subject to} \quad \mathbb{E}_{\mathbf{b}, \mathbf{n}_1, \mathbf{n}_2} \left[\sum_{k=1}^N |x[k]|^2 \right] \leq N \quad (7)$$

The expectation in (7) is taken over the distributions of the bit stream \mathbf{b} and the noises, \mathbf{n}_1 and \mathbf{n}_2 , since the encoding output $x[k]$ depends on \mathbf{b} , \mathbf{n}_1 , and \mathbf{n}_2 in (4), where $\mathbf{n}_1 = [n_1[1], \dots, n_1[N]]^T$ and $\mathbf{n}_2 = [n_2[1], \dots, n_2[N]]^T$.

Thus, the goal is to optimize N encoding functions $\{f_k\}_{k=1}^N$ and a decoding function g . However, the complexity of designing N encoding functions increases to a great extent with the number of channel uses N . To mitigate the associated design complexity, we introduce a state propagation-based encoding technique, discussed next.

2.4. State Propagation-Based Encoding

Given that the inputs used for encoding at each time in (4) are overlapping, we expect that the N encoding functions are correlated with one another. As a result, we consider a state propagation-based encoding technique where the encoding is performed at each timestep using only two distinct functions: (i) signal-generation and (ii) state-propagation.

Defining the signal-generation function as $f : \mathbb{R}^{K+N_s+1} \rightarrow \mathbb{R}$, we re-write the encoding process in (4) as

$$x[k] = f(\mathbf{b}, z[k-1], \mathbf{s}[k]), \quad k = 1, \dots, N, \quad (8)$$

where we assume $z[-1] = 0$. Here, $\mathbf{s}[k] \in \mathbb{R}^{N_s}$ is the state vector, which propagates over time through the state-propagation function $h : \mathbb{R}^{K+N_s+1} \rightarrow \mathbb{R}^{N_s}$, given by

$$\mathbf{s}[k] = h(\mathbf{b}, z[k-1], \mathbf{s}[k-1]), \quad k = 1, \dots, N. \quad (9)$$

Note that, in (9), the current state $\mathbf{s}[k]$ is updated from the prior state $\mathbf{s}[k-1]$ by incorporating \mathbf{b} and $z[k-1]$. For the initial condition, we assume $\mathbf{s}[-1] = \mathbf{0}$. This encoding

model in (8)-(9) can be seen as a general and non-linear extension of the state-space model used for linear encoding in feedback systems (Elia, 2004).

Through this technique, we only need to design the two encoding functions, f and h – instead of N separate functions – and the decoding function g . We thus re-write the optimization problem in (6)-(7) as

$$\underset{f, h, g}{\text{minimize}} \quad \Pr[\mathbf{b} \neq \hat{\mathbf{b}}] \quad (10)$$

$$\text{subject to} \quad \mathbb{E}_{\mathbf{b}, \mathbf{n}_1, \mathbf{n}_2} \left[\sum_{k=1}^N |x[k]|^2 \right] \leq N. \quad (11)$$

Nevertheless, the problem (10)-(11) is non-trivial since the functions, f , h , and g , can take arbitrary forms. Over several decades of research in the design of such functions, a linear assumption was made (Schalkwijk & Kailath, 1966; Butman, 1969; Chance & Love, 2011).¹ While omitting low-complexity schemes, this constrains the degree of freedom in the design of such functions, leading to unsatisfactory error performances (Kim et al., 2018a). We next employ this state propagation-based encoding in the design of non-linear feedback codes that are robust to channel noise.

3. Feedback Coding Methodology

Our overall coding scheme is depicted in Figure 2. It follows the RNN autoencoder-based architecture detailed below.

3.1. Encoding

We follow the state propagation-based encoding approach discussed in Section 2.4. The state-propagation function h in (9) consists of two layers of gated recurrent units (GRUs), while the signal-generation function f in (8) consists of a non-linear layer and a power control layer in sequence.

GRUs for state propagation. We adopt two layers of uni-directional GRUs to capture the time correlation of the feedback signals in a causal manner. Formally, we represent the input-output relationship at each layer at time k as

$$\mathbf{s}_1[k] = \text{GRU}_1(\mathbf{b}, z[k-1], \mathbf{s}_1[k-1]), \quad (12)$$

$$\mathbf{s}_2[k] = \text{GRU}_2(\mathbf{s}_1[k], \mathbf{s}_2[k-1]), \quad (13)$$

where GRU_i represents a functional form of GRU processing at layer i and $\mathbf{s}_i[k] \in \mathbb{R}^{N_{s,i}}$ is the state vector obtained by GRU_i at time k , where $i = 1, 2$ and $k = 1, \dots, N$. For the initial conditions, we assume $\mathbf{s}_i[-1] = \mathbf{0}$, $i = 1, 2$.

(12)-(13) can be represented as a functional form of the state propagation-based encoding in (9). By defining the overall state vector as $\mathbf{s}[k] = [\mathbf{s}_1[k], \mathbf{s}_2[k]]$, we obtain $\mathbf{s}[k] =$

$h(\mathbf{b}, z[k-1], \mathbf{s}[k-1])$, where h implies the process of two layers of GRUs in (12)-(13). Note that $\mathbf{s}[k]$ propagates over time through the GRUs by incorporating the current input information into its state. Because the bit stream \mathbf{b} with length K is handled as a *block* to generate transmit signals with any length N , our method is flexible enough to support any coding rate r , unlike the prior approach (Kim et al., 2018a) that only appears to support $r = 1/3$.

Non-linear layer. We consider that only the state vector at the last layer, i.e., $\mathbf{s}_2[k]$, is taken as an input to the non-linear layer. Formally, we can represent the process of the non-linear layer as

$$\tilde{x}[k] = \phi(\mathbf{w}_e^T \mathbf{s}_2[k] + b_e), \quad k = 1, \dots, N, \quad (14)$$

where $\mathbf{w}_e \in \mathbb{R}^{N_{s,2}}$ and $b_e \in \mathbb{R}$ are the trainable weights and biases, respectively, and $\phi : \mathbb{R} \rightarrow \mathbb{R}$ is an activation function (hyperbolic tangent).

It is possible to use $\tilde{x}[k]$ directly as a transmit signal, since $\tilde{x}[k]$ ranges in $(-1, 1)$ and satisfies the power constraint $\sum_{k=1}^N |\tilde{x}[k]|^2 \leq N$. However, this does not ensure maximum utilization of the transmit power budget. Power control over the sequence of transmit signals is essential in the design of encoding schemes for feedback-enabled communications in order to achieve robust error performance (Schalkwijk & Kailath, 1966; Chance & Love, 2011; Kim et al., 2018a).

Power control layer. We introduce a power control layer to optimize for the power distribution, while also satisfying the power constraint in (11). This layer consists of two consecutive modules: (i) normalization and (ii) power-weight multiplication. The transmit signal at time k is then generated by

$$x[k] = w_k \gamma_k^{(J)}(\tilde{x}[k]), \quad k = 1, \dots, N, \quad (15)$$

where $\gamma_k^{(J)} : \mathbb{R} \rightarrow \mathbb{R}$ is a normalization function applied to $\tilde{x}[k]$, which consists of the sample mean and sample variance calculated from the data with size J . Here, w_k is a trainable power weight satisfying $\sum_{k=1}^N w_k^2 = N$.

Through the power control layer, the power weights are optimized via training in a way that minimizes the BLER in (10). At the same time, the power constraint in (11) should be satisfied. To obtain a smaller BLER, it is advantageous to ensure maximum utilization of the power budget N (Schalkwijk & Kailath, 1966; Chance & Love, 2011). However, satisfying the power constraint in an (ensemble) average sense is non-trivial, since the distributions of $\{x[k]\}_{k=1}^N$ are unknown. Therefore, we approach it in an empirical sense: (i) During training, we normalize $\tilde{x}[k]$ with the sample mean and sample variance calculated from each batch of data (with size N_{batch}) at each k . (ii) After training, we calculate and save the sample mean and sample variance from

¹The existing works, such as SK, CL, and Deepcode, can be interpreted in the framework of state propagation-based encoding.

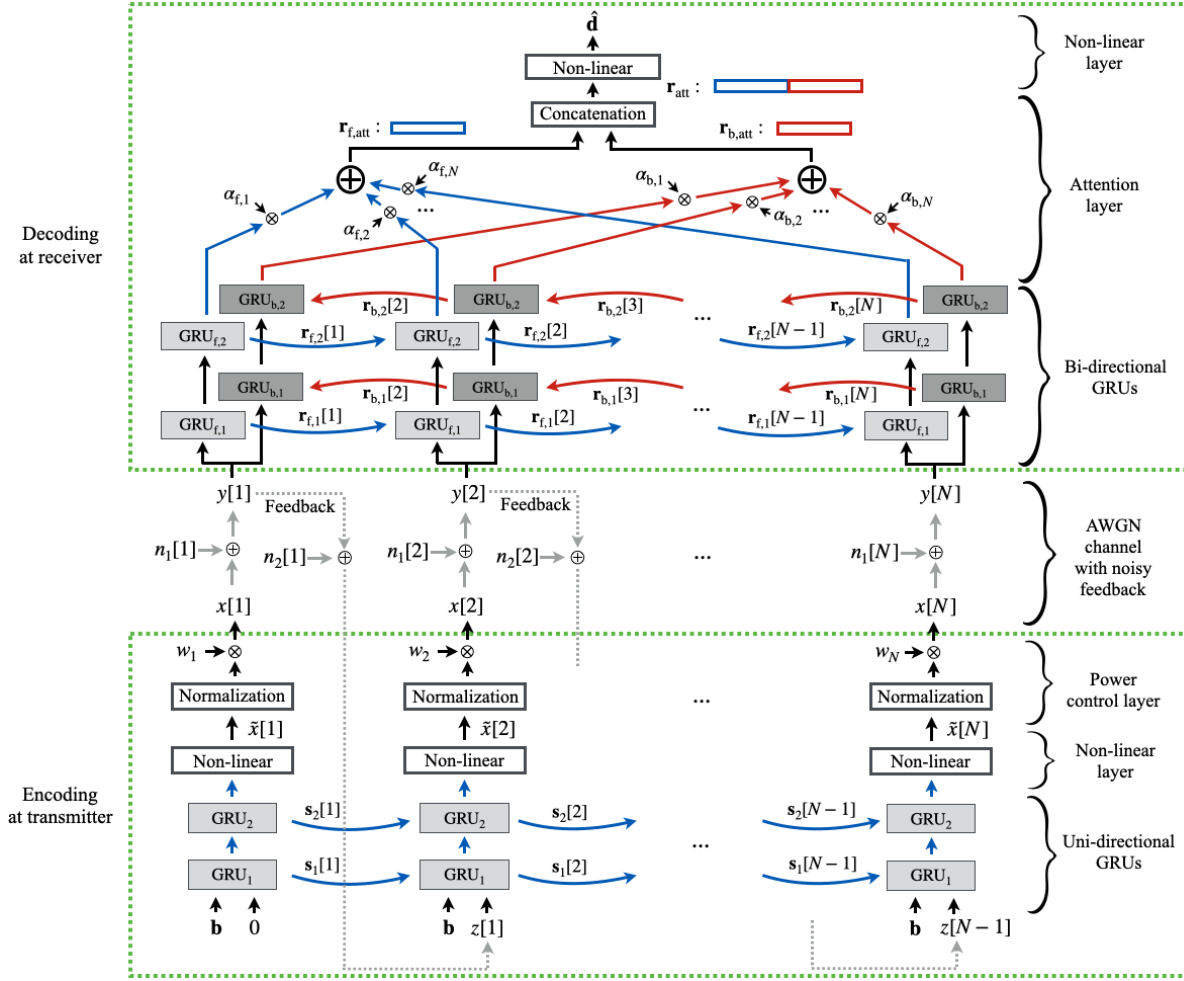


Figure 2. Our proposed RNN autoencoder-based architecture for non-linear coding over an AWGN channel with noisy feedback. A compact form of the architecture is included in Appendix C.

the entire training data (with size J). (iii) For inference, we use the saved mean and variance for normalization.

In the following lemma, we show that the above procedure guarantees satisfaction of the equality power constraint in an asymptotic sense with a large number of training data used for normalization.

Lemma 1. *Given the power control layer in (15), the power constraint in (11) converges to N almost surely, i.e., $\mathbb{E}_{\mathbf{b}, \mathbf{n}_1, \mathbf{n}_2} [\sum_{k=1}^N |x[k]|^2] \xrightarrow{a.s.} N$, as the number of training data J used for normalization tends to infinity.*

Proof. See Appendix A. \square

Remark 1. Because of the data-dependent normalization in generating $x[k]$ in (15), $\mathbb{E}_{\mathbf{b}, \mathbf{n}_1, \mathbf{n}_2} [\sum_{k=1}^N |x[k]|^2]$ is a random sequence along J in our implementation. We note that our neural network builds resiliency to the small size of inference data by using the saved mean and variance (rather than calculating them with the batch of inference data).

3.2. Decoding

As shown in Figure 2, our decoding function g consists of the bi-directional GRUs, the attention layer, and the non-linear layer. We discuss each of them in detail below.

Bi-directional GRU. We utilize two layers of bi-directional GRUs to capture the time correlation of the receive signals both in the forward and backward directions. We represent the input-output relationship of the forward directional GRUs at time k as

$$\begin{aligned} \mathbf{r}_{f,1}[k] &= \text{GRU}_{f,1}(y[k], \mathbf{r}_{f,1}[k-1]), \\ \mathbf{r}_{f,2}[k] &= \text{GRU}_{f,2}(\mathbf{r}_{f,1}[k], \mathbf{r}_{f,2}[k-1]), \end{aligned} \quad (16)$$

and that of the backward directional GRUs as

$$\begin{aligned} \mathbf{r}_{b,1}[k] &= \text{GRU}_{b,1}(y[k], \mathbf{r}_{b,1}[k+1]), \\ \mathbf{r}_{b,2}[k] &= \text{GRU}_{b,2}(\mathbf{r}_{b,1}[k], \mathbf{r}_{b,2}[k+1]), \end{aligned} \quad (17)$$

where $\text{GRU}_{f,i}$ and $\text{GRU}_{b,i}$ represent functional forms of GRU at layer i in the forward and backward direction, re-

spectively. Here, $\mathbf{r}_{f,i}[k] \in \mathbb{R}^{N_{r,i}}$ and $\mathbf{r}_{b,i}[k] \in \mathbb{R}^{N_{r,i}}$ are the state vectors obtained by $\text{GRU}_{f,i}$ and $\text{GRU}_{b,i}$, respectively, at time k , where $i = 1, 2$ and $k = 1, \dots, N$. For the initial conditions, $\mathbf{r}_{f,i}[-1] = \mathbf{0}$ and $\mathbf{r}_{b,i}[N+1] = \mathbf{0}$, $i = 1, 2$.

Attention layer. We consider the state vectors at the last layer, i.e., $\mathbf{r}_{f,2}[k]$ and $\mathbf{r}_{b,2}[k]$, over $k = 1, \dots, N$, as inputs to the attention layer. Each state vector contains different feature information depending on both its direction and time-step k : The forward state vector $\mathbf{r}_{f,2}[k]$ captures the implicit correlation information of the receive signals of $y[1], \dots, y[k]$, while the backward state vector $\mathbf{r}_{b,2}[k]$ captures that of $y[k], \dots, y[N]$, $k = 1, \dots, N$. Although the state vectors at each end, i.e., $\mathbf{r}_{f,2}[N]$ and $\mathbf{r}_{b,2}[1]$, contain the information of all receive signals, the long-term dependency cannot be fully captured (Bengio et al., 1993). Therefore, we adopt the attention layer (Bahdanau et al., 2014). Formally,

$$\mathbf{r}_{f,\text{att}} = \sum_{k=1}^N \alpha_{f,k} \mathbf{r}_{f,2}[k], \quad \mathbf{r}_{b,\text{att}} = \sum_{k=1}^N \alpha_{b,k} \mathbf{r}_{b,2}[k], \quad (18)$$

where $\alpha_{f,k} \in \mathbb{R}$ and $\alpha_{b,k} \in \mathbb{R}$ are the trainable *attention weights* applied to the forward and backward state vectors, respectively, $k = 1, \dots, N$. To capture the forward and backward directional information separately, we stack the two vectors, leading to

$$\mathbf{r}_{\text{att}} = [\mathbf{r}_{f,\text{att}}^T, \mathbf{r}_{b,\text{att}}^T]^T. \quad (19)$$

In this separated encoder-decoder architecture, the attention mechanism at the decoder enables the decoder to fully exploit the noisy signal information $\{y[k]\}_{k=1}^N$.

Non-linear layer. At the end of the decoder, we utilize a non-linear layer to finally obtain the estimate $\hat{\mathbf{b}}$ by using the feature vector \mathbf{r}_{att} in (19). The input-output relationship at the non-linear layer is given by

$$\hat{\mathbf{d}} = \theta(\mathbf{W}_d \mathbf{r}_{\text{att}} + \mathbf{v}_d) \quad (20)$$

where $\theta : \mathbb{R}^{2N_{r,2}} \rightarrow \mathbb{R}^M$ is an activation function $\mathbf{W}_d \in \mathbb{R}^{M \times 2N_{r,2}}$ and $\mathbf{v}_d \in \mathbb{R}^M$ are the trainable weights and biases, respectively. In this work, we consider softmax function for θ and set to $M = 2^K$. Then, $\hat{\mathbf{d}} \in \mathbb{R}^{2^K}$ denotes the probability distribution of 2^K possible outcomes of $\hat{\mathbf{b}}$.

Model training and inference. For training, we consider the cross entropy (CE) loss $\text{CE}(\mathbf{d}, \hat{\mathbf{d}}) = -\sum_{i=1}^{2^K} d_i \log \hat{d}_i$, where $\mathbf{d} \in \{0, 1\}^{2^K}$ is the one-hot representation of $\mathbf{b} \in \{0, 1\}^K$, and d_i and \hat{d}_i are the i -th entry of \mathbf{d} and $\hat{\mathbf{d}}$, respectively. For inference, we force the entry with the largest value of $\hat{\mathbf{d}}$ to 1, while setting the rest of the entries to 0, and then map the obtained one-hot vector to a bit stream vector $\hat{\mathbf{b}}$. By treating the entire bit stream as a block through the use of one-hot vectors, we transform our problem of minimizing BLER, i.e., $\Pr[\mathbf{b} \neq \hat{\mathbf{b}}]$ in (10), into a classification problem.

3.3. Performance-Complexity Tradeoff

In our scheme, the encoder and decoder will have computational complexities of $\mathcal{O}(N_e^2 N)$ and $\mathcal{O}(N_d^2 N + N_d 2^K)$, respectively, assuming that the same number of neurons, N_e and N_d , is used at each layer of the encoder and decoder. The linear coding scheme, such as CL, only requires $\mathcal{O}(N^2)$ and $\mathcal{O}(N)$ at the encoder and decoder, respectively. On the other hand, for the error correction codes, decoding often imposes high computation overhead. For example, turbo decoder typically needs more than 10 iterations, each followed by a permutation. It is important to note that the computations in our scheme are mostly matrix calculations, which allows them to be parallelized. Overall, given the trade-off between performance and complexity, we can consider our non-linear feedback coding to improve the communication reliability at the expense of higher complexity compared with linear schemes.

4. Experimental Results

We now present numerical experiments to validate our methodology. We measure noise power and signal to noise ratio (SNR) in decibels (dB). For brevity, details on our training procedure are relegated to Appendix B.

4.1. Baselines

We consider several baselines including state-of-the-art feedback schemes and well-known error correction codes.

Repetition coding: Each bit of $\mathbf{b} \in \{0, 1\}^K$ is modulated with binary phase-shift keying (BPSK) and transmitted repetitively over N/K channel uses.

TBCC (Ma & Wolf, 1986): We consider tail-biting convolutional coding (TBCC), adopted in LTE standards (3GPP TS 36.212, 2010) for short blocklength codes. We consider the trellis with (7, [133, 171, 165]) and BPSK modulation.

Turbo coding (Berrou & Glavieux, 1996): We consider turbo codes, adopted in LTE standards for medium/long blocklength codes. We consider the trellis with (4, [13, 15]), BPSK modulation, and 10 decoding iterations.

CL scheme with 2^B -ary PAM (Chance & Love, 2011): The bit stream \mathbf{b} is first divided into K/B bit chunks each with length B . Each bit chunk is modulated with 2^B -ary pulse amplitude modulation (PAM), and then transmitted over NB/K channel uses with the CL scheme.

Deepcode (Kim et al., 2018a): This is a non-linear feedback coding scheme that uses RNNs to encode/decode the bit stream \mathbf{b} based on a bit-by-bit processing.

TBCC with CL: This is a concatenated coding approach with TBCC for outer coding and the CL scheme for inner coding. The bit stream \mathbf{b} is encoded with TBCC to generate

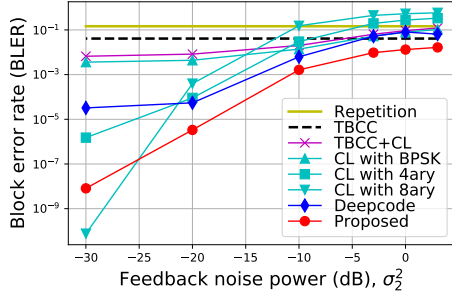


Figure 3. BLER with short blocklength $K = 6$ and rate $r = 1/3$ when the forward SNR is 1dB. Our feedback codes outperform the counterparts and demonstrate robustness to high feedback noise.

the outer code $\mathbf{c} \in \{0, 1\}^{K/r_{\text{out}}}$ with outer coding rate $r_{\text{out}} = 1/2$ and the trellis with $(7, [133, 171])$. \mathbf{c} is modulated with 2^B -ary PAM where $B = 2$, and each symbol is transmitted with the CL scheme over $N r_{\text{out}} B / K$ channel uses.

Turbo with CL: This is a concatenated coding approach where turbo coding is used for outer coding. For turbo coding, we consider $r_{\text{out}} = 1/3$, the trellis with $(4, [13, 15])$, and 10 decoding iterations. For the CL scheme as inner coding, we consider 2^B -ary PAM where $B = 2$.

4.2. Short Blocklength

We first investigate our approach under a short blocklength regime. Figure 3 shows BLER curves along varying feedback noise powers, where $K = 6$ and $N = 18$ with rate $r = 1/3$ and a forward SNR of 1dB ($\sigma_1^2 = 0.794$). Due to the lack of feedback usage, the repetition coding and TBCC provide constant BLERs along the feedback noise powers, whereas the feedback schemes, such as Deepcode, CL, and our scheme, perform better as the feedback becomes less noisy. Over all reasonable feedback noise regions, our scheme outperforms the alternatives, usually by more than 5dB. Importantly, as the feedback noise increases to higher levels, i.e., $\sigma_2^2 \geq -5$ dB, our scheme still improves the BLER performance by several dB when compared to TBCC, whereas other feedback codes are shown to be much more vulnerable to high feedback noise. This validates the improvement in resilience to feedback noise that our scheme achieves. When the feedback noise becomes extremely large, our scheme behaves like an open-loop code rather than feedback codes, further demonstrated in Appendix D.1. Also, the results with various selections of K and r are consistent with the ones obtained from Figure 3, which are included in Appendix D.2.

4.3. Extension to Medium/Long Blocklength

We next consider a medium/long blocklength regime with rate $r = 1/3$ and blocklength L . The feedback schemes can

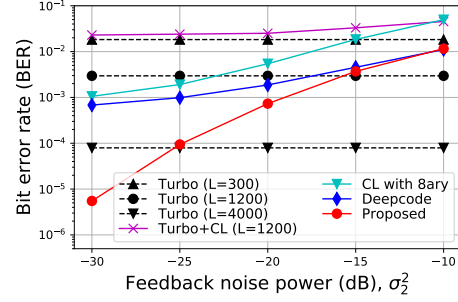


Figure 4. BER with medium/long blocklength L and rate $r = 1/3$ when the forward SNR is low (-1 dB). Our feedback codes significantly improve BER performances compared to other feedback schemes over a wide range of feedback noise powers.

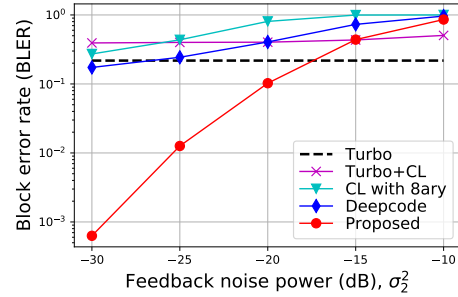


Figure 5. BLER with medium blocklength $L = 300$ and rate $r = 1/3$ when the forward SNR is -1 dB. Our scheme provides a greatly enhanced region where turbo codes are outperformed.

be straightforwardly extended to the medium/long blocklength codes in a time division manner; a total of L bits are divided into L/K chunks of bits, and each chunk with length K is processed with feedback schemes.² We consider our scheme with $K = 6$ and Deepcode with $K = 10$.³

Figure 4 shows bit error rate (BER) performances in the high forward noise scenario where the forward SNR is -1 dB ($\sigma_1^2 = 1.26$). Due to the time division processing of the feedback schemes including our scheme, Deepcode, and CL, the obtained BERs are the same for different choices of blocklength L , while turbo coding benefits from the longer blocklength. Given blocklength L , we identify a feedback noise power threshold, below which feedback schemes outperform turbo coding. We observe that, in this high forward noise scenario, our scheme benefits significantly from lower feedback noise power, while other feedback codes do not.

Figure 5 shows BLERs with medium blocklength $L = 300$ where the forward SNR is -1 dB. Our scheme provides a better threshold while outperforming the other feedback

²Although our feedback scheme can be used as inner coding for concatenated coding with a flexible inner coding rate, this strategy does not yield satisfactory results in BER and BLER for $r = 1/3$. For Deepcode, outer coding is not allowed for rate $1/3$.

³For Deepcode, other choices of K yield similar performances.

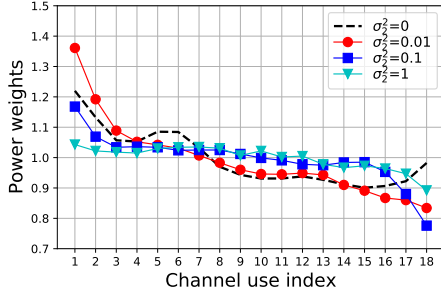


Figure 6. Transmit power distribution over $N = 18$ channel uses. The power values are larger at the beginning, and decrease along the channel uses, which aligns with the result of the CL scheme.

techniques by more than two orders of magnitude in BLER. Consistent results are observed over a variety of selections of L , which are presented in Appendix D.3. Nevertheless, in a very long blocklength regime, e.g., $L = 4000$, turbo code may be still preferable to feedback codes unless the feedback noise is low enough, as shown in Figure 4.

4.4. Power Control in Encoding

Figure 6 shows the power weights obtained by our scheme, $\{w_k\}_{k=1}^N$ in (15), over $N = 18$ channel uses, under different feedback noise power scenarios. We consider $K = 6$, $r = 1/3$, and a forward SNR of 1dB. When feedback is available, the power allocation along the channel uses becomes uneven, with more powers being allocated at the start and less being distributed along later channel uses. This result aligns with the power distribution obtained by the optimized CL linear feedback coding scheme under noisy feedback. This demonstrates that regardless of whether the encoding and decoding process is linear or non-linear, more powers should be allocated at the beginning to maximize the use of the feedback information under noisy feedback. The power distribution obtained by the CL scheme and further discussion on these points are included in Appendix E.

4.5. Attention Mechanism in Decoding

Figure 7 shows the attention weights for forward and backward directions, $\{\alpha_{f,k}\}_{k=1}^N$ and $\{\alpha_{b,k}\}_{k=1}^N$ in (18), along $N = 18$ channel uses under various feedback noise power scenarios. We consider $K = 6$, $r = 1/3$, and a forward SNR of 1dB. For the low noise power scenarios, i.e., $\sigma_2^2 = 0.01$ or 0.1 , there is an overlap of the non-zero weight regions for forward and backward directions. This implies that all the receive signals, $y[1], \dots, y[N]$, are utilized at the decoder since $\alpha_{f,k} > 0$ means that the decoder captures the features of the receive signals, $y[1], \dots, y[k]$, through the forward GRUs, while $\alpha_{b,k} > 0$ means that the decoder captures the features of $y[k], \dots, y[N]$ through the backward GRUs. On the other hand, with high feedback noise, i.e., $\sigma_2^2 = 1$,

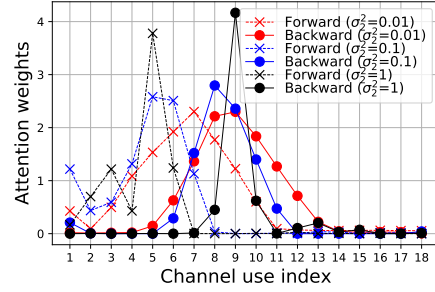


Figure 7. Bi-directional attention weights along channel uses. Through the bi-directional GRUs and attention weights, the decoder aims to fully leverage the receive signals.

we have $\alpha_{f,k} = \alpha_{b,k} \approx 0$ at $k = 7$, indicating that the receive signal $y[7]$ would not be used at the decoder. However, it is important to note that some information of $y[7]$ is contained in the next-time signals, $y[k]$, $k = 8, 9, \dots, N$ due to the causal encoding process that uses feedback signals as an input. As a result, for all noise conditions, it is expected that the decoder will attempt to fully leverage the correlation of the receive signals to reconstruct the original bit stream.

Appendix F contains a number of ablation studies and simulations performed under various configurations, which are consistent with the findings in this section.

5. Conclusion

In this work, we presented a new class of non-linear feedback codes that significantly increase robustness against channel noise via a novel RNN autoencoder architecture. Our learning architecture addressed the challenges of encoder-decoder separation over a noisy channel and inefficient power allocation. To overcome encoder-decoder separation, we processed the entire bit stream as a single unit to benefit from noise averaging, and adopted a bi-directional attention-based decoding architecture to fully exploit correlations among noisy receive signals. For power optimization, we introduced a power control layer at the encoder, and proved that the power constraint is satisfied asymptotically. Through numerical experiments, we demonstrated that under realistic forward/feedback noise regimes, our scheme outperforms state-of-the-art feedback codes significantly. We also provided information-theoretic insights on the power distribution of our non-linear feedback codes, showing that allocated power decreases over time.

One other important observation we made is that canonical error correction codes still outperform feedback schemes when the feedback noise becomes high in a long blocklength regime. In future work, it will be interesting to further investigate the joint characteristics of our feedback codes in terms of error correction coding and feedback coding as mentioned in Appendix D.1 to adapt to noise conditions.

References

- 3GPP TS 36.212. LTE: Evolved universal terrestrial radio access (E-UTRA): Multiplexing and channel coding. V8.8.0 Release 8, 2010.
- Agrawal, M., Love, D. J., and Balakrishnan, V. An iteratively optimized linear coding scheme for correlated Gaussian channels with noisy feedback. In *49th Annual Allerton Conference on Communication, Control, and Computing*, pp. 1012–1018. IEEE, 2011.
- Bahdanau, D., Cho, K., and Bengio, Y. Neural machine translation by jointly learning to align and translate. *arXiv preprint arXiv:1409.0473*, 2014.
- Ben-Yishai, A. and Shayevitz, O. Interactive schemes for the AWGN channel with noisy feedback. *IEEE Transactions on Information Theory*, 63(4):2409–2427, 2017.
- Bengio, Y., Frasconi, P., and Simard, P. The problem of learning long-term dependencies in recurrent networks. In *IEEE international conference on neural networks*, pp. 1183–1188. IEEE, 1993.
- Berrou, C. and Glavieux, A. Near optimum error correcting coding and decoding: Turbo-codes. *IEEE Transactions on communications*, 44(10):1261–1271, 1996.
- Butman, S. A general formulation of linear feedback communication systems with solutions. *IEEE Transactions on Information Theory*, 15(3):392–400, 1969.
- Chance, Z. and Love, D. J. Concatenated coding for the AWGN channel with noisy feedback. *IEEE Transactions on Information Theory*, 57(10):6633–6649, 2011.
- Chen, X. and Ye, M. Cyclically equivariant neural decoders for cyclic codes. *arXiv preprint arXiv:2105.05540*, 2021.
- Clark Jr, G. C. and Cain, J. B. *Error-correction coding for digital communications*. Springer Science & Business Media, 2013.
- Dörner, S., Cammerer, S., Hoydis, J., and Ten Brink, S. Deep learning based communication over the air. *IEEE Journal of Selected Topics in Signal Processing*, 12(1): 132–143, 2017.
- Elia, N. When Bode meets Shannon: Control-oriented feedback communication schemes. *IEEE transactions on Automatic Control*, 49(9):1477–1488, 2004.
- Habib, S., Beemer, A., and Kliwer, J. Learning to decode: Reinforcement learning for decoding of sparse graph-based channel codes. *Advances in neural information processing systems*, 33:22396–22406, 2020.
- Jiang, Y., Kim, H., Asnani, H., Kannan, S., Oh, S., and Viswanath, P. Turbo autoencoder: Deep learning based channel codes for point-to-point communication channels. *Advances in neural information processing systems*, 32, 2019.
- Kim, H., Jiang, Y., Kannan, S., Oh, S., and Viswanath, P. Deepcode: Feedback codes via deep learning. *Advances in neural information processing systems*, 31, 2018a.
- Kim, H., Jiang, Y., Rana, R., Kannan, S., Oh, S., and Viswanath, P. Communication algorithms via deep learning. *arXiv preprint arXiv:1805.09317*, 2018b.
- Ma, H. and Wolf, J. On tail biting convolutional codes. *IEEE Transactions on Communications*, 34(2):104–111, 1986.
- Makkuva, A. V., Liu, X., Jamali, M. V., MahdaviFar, H., Oh, S., and Viswanath, P. Ko codes: inventing nonlinear encoding and decoding for reliable wireless communication via deep-learning. In *International Conference on Machine Learning*, pp. 7368–7378. PMLR, 2021.
- Mishra, R., Vasal, D., and Kim, H. Linear coding for AWGN channels with noisy output feedback via dynamic programming. In *IEEE International Symposium on Information Theory (ISIT)*, pp. 13–18, July 2021.
- Nachmani, E., Be’ery, Y., and Burshtein, D. Learning to decode linear codes using deep learning. In *2016 54th Annual Allerton Conference on Communication, Control, and Computing (Allerton)*, pp. 341–346. IEEE, 2016.
- Ozfatura, E., Shao, Y., Perotti, A., Popovic, B., and Gündüz, D. All you need is feedback: Communication with block attention feedback codes. *IEEE Journal on Selected Areas in Information Theory*, 2022.
- O’shea, T. and Hoydis, J. An introduction to deep learning for the physical layer. *IEEE Transactions on Cognitive Communications and Networking*, 3(4):563–575, 2017.
- Schalkwijk, J. and Kailath, T. A coding scheme for additive noise channels with feedback–i: No bandwidth constraint. *IEEE Transactions on Information Theory*, 12(2):172–182, 1966.
- Shafi, M., Molisch, A. F., Smith, P. J., Haustein, T., Zhu, P., De Silva, P., Tufvesson, F., Benjebbour, A., and Wunder, G. 5G: A tutorial overview of standards, trials, challenges, deployment, and practice. *IEEE journal on selected areas in communications*, 35(6):1201–1221, 2017.
- Shannon, C. The zero error capacity of a noisy channel. *IRE Transactions on Information Theory*, 2(3):8–19, 1956.
- Shannon, C. E. A mathematical theory of communication. *The Bell system technical journal*, 27(3):379–423, 1948.

Shayevitz, O. and Feder, M. Optimal feedback communication via posterior matching. *IEEE Transactions on Information Theory*, 57(3):1186–1222, 2011.

A. Proof of Lemma 1

Proof. Define the training data tuples as $\{\mathcal{T}_j\}_{j=1}^J$ where $\mathcal{T}_j = \{\hat{\mathbf{b}}^{(j)}, \hat{\mathbf{n}}_1^{(j)}, \hat{\mathbf{n}}_2^{(j)}\}$. Let us denote $\tilde{\eta}_j[k]$ as the output at timestep k generated by data j , \mathcal{T}_j , through the encoding process of (12)-(14), $k = 1, \dots, N$. It is obvious that $\tilde{\eta}_j[k]$ is independent and identically distributed (i.i.d.) over j assuming the data tuples $\{\mathcal{T}_j\}_{j=1}^J$ are i.i.d. from each other. We define the mean and variance of $\tilde{\eta}_j[k]$ as μ_k and σ_k^2 , respectively. With the sample mean $m_k(J) = \frac{1}{J} \sum_{j=1}^J \tilde{\eta}_j[k]$ and the sample variance $\delta_k^2(J) = \frac{1}{J} \sum_{j=1}^J (\tilde{\eta}_j[k] - m_k(J))^2$, we define the normalization function as $\gamma_k^{(J)}(x) = (x - m_k(J))/\delta_k(J)$.

Let us define $\tilde{x}[k]$ as the output at timestep k generated by the data tuple for inference, $\{\mathbf{b}, \mathbf{n}_1, \mathbf{n}_2\}$. Assuming the training and inference data tuples are extracted from the same distribution, the mean and variance of $\tilde{x}[k]$ are then μ_k and σ_k^2 , respectively. We then have $\mathbb{E}_{\mathbf{b}, \mathbf{n}_1, \mathbf{n}_2} [|\gamma_k^{(J)}(\tilde{x}[k])|^2] = \frac{\sigma_k^2 + (m_k(J) - \mu_k)^2}{\delta_k^2(J)}$. By strong law of large number (SLLN), $m_k(J) \rightarrow \mu_k$ and $\delta_k^2(J) \rightarrow \sigma_k^2$ almost surely (a.s.) as $J \rightarrow \infty$. Then, by continuous mapping theorem, $\mathbb{E}_{\mathbf{b}, \mathbf{n}_1, \mathbf{n}_2} [|\gamma_k^{(J)}(\tilde{x}[k])|^2] \rightarrow 1$ a.s. as $J \rightarrow \infty$. Then, $\mathbb{E}_{\mathbf{b}, \mathbf{n}_1, \mathbf{n}_2} [\sum_{k=1}^N |x[k]|^2] = \sum_{k=1}^N w_k^2 \mathbb{E}_{\mathbf{b}, \mathbf{n}_1, \mathbf{n}_2} [|\gamma_k^{(J)}(\tilde{x}[k])|^2] \rightarrow N$ a.s. as $J \rightarrow \infty$. \square

B. Parameter Setup and Algorithm for Training

The overall algorithm for training is given in Algorithm 1. The number of training data is $J = 10^7$, the batch size is $N_{\text{batch}} = 2.5 \times 10^4$, and the number of epochs is $N_{\text{epoch}} = 100$. We use the Adam optimizer and a decaying learning rate, where the initial rate is 0.01 and the decaying ratio is $\gamma = 0.95$ applied for every epoch. We also use gradient clipping for training, where the gradients are clipped when the norm of gradients is larger than 1. We adopt two layers of uni-directional GRUs at the encoder and two layers of bi-directional GRUs at the decoder, with $N_{\text{neurons}} = 50$ neurons at each GRU. We initialize each neuron in GRUs with $U(-1/\sqrt{N_{\text{neurons}}}, 1/\sqrt{N_{\text{neurons}}})$, and all the power weights and attention weights to 1. We train our neural network model under particular forward/feedback noise powers and conduct inference in the same noise environment.

Algorithm 1 Training for the proposed RNN autoencoder-based architecture

Input: Training data $\{\mathbf{b}^{(j)}, \mathbf{n}_1^{(j)}, \mathbf{n}_2^{(j)}\}_{j=1}^J$, number of epochs N_{epoch} , and batch size N_{batch} .

Output: Model parameters

Initialize the model parameters.

for $e = 1$ **to** N_{epoch} **do**

for $t = 1$ **to** J/N_{batch} **do**

 Obtain N_{batch} data tuples, $\{\mathbf{b}^{(\ell)}, \mathbf{n}_1^{(\ell)}, \mathbf{n}_2^{(\ell)}\}_{\ell \in \mathcal{I}_{\text{batch}}}$, where $\mathcal{I}_{\text{batch}}$ denotes the indices of the extracted data tuples with $|\mathcal{I}_{\text{batch}}| = N_{\text{batch}}$.

 Update the model parameters using the gradient decent on the cross entropy loss, defined by $\sum_{\ell \in \mathcal{I}_{\text{batch}}} \text{CE}(\mathbf{d}^{(\ell)}, \hat{\mathbf{d}}^{(\ell)}) = -\sum_{\ell \in \mathcal{I}_{\text{batch}}} \sum_{i=1}^{2^K} d_i^{(\ell)} \log \hat{d}_i^{(\ell)}$, where $\mathbf{d}^{(\ell)} = \text{one-hot}(\mathbf{b}^{(\ell)})$ is the target vector, and $\hat{\mathbf{d}}^{(\ell)}$ is the output obtained by the ℓ -th data tuple passing through the overall encoder-decoder architecture in (12)-(20).

end for

end for

C. Encoder and Decoder in a Compact Form

Figure 8 shows a compact version of the encoder and decoder, where a unrolled version along timesteps is demonstrated in Figure 2. The encoder and decoder are present at the transmitter and receiver, respectively, under the framework of autoencoder architectures. The encoding output $x[k]$ travels through a noisy channel, and the noisy version of $x[k]$, i.e., $y[k]$, is provided as an input to the decoder. Our goal with this RNN autoencoder-based structure is to jointly train the encoder and decoder.

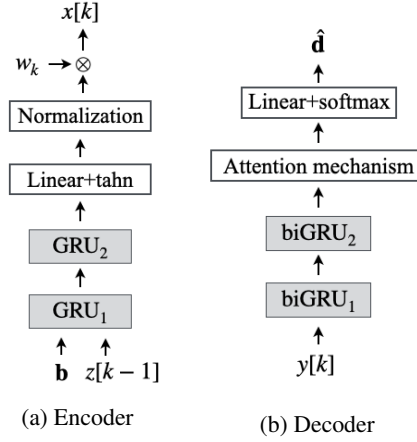


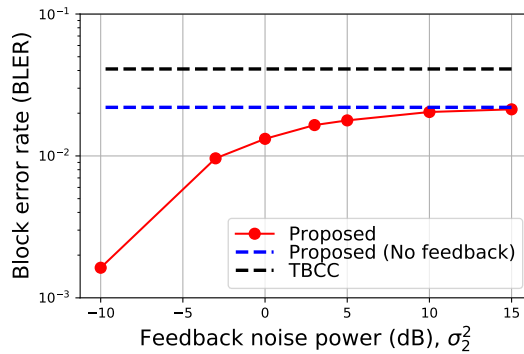
Figure 8. Encoder and decoder in a compact structure.

D. Evaluations of Our Scheme under Various Scenarios

D.1. Adaptability of our method to feedback noise

Figure 9 shows the BLER curves for the region of high feedback noise powers. We consider $K = 6$, $N = 18$, and the forward SNR with 1dB. Our learning architecture shown in Figure 2 can be modified to generate an open-loop code that does not use any feedback signals at all, by providing $x[k]$ as an input to the encoder rather than $z[k]$. This open-loop code, denoted by Proposed (No feedback) in Figure 9, outperforms TBCC, showing that our learning architecture may be utilized to create error correction codes. While keeping this as a prospective research area for future works on error correction coding, we are more interested in the behavior of our scheme in terms of feedback utilization in this work.

It is interesting that as the feedback noise power increases, the performance of our original method (using feedback) converges to the one of our open-loop coding (without feedback utilization). In contrast, as the feedback becomes less noisy, our scheme beats our open-loop coding scheme by maximizing the use of the feedback information. This demonstrates the adaptability of our approach, which may weight feedback coding or open-loop coding differently depending on the feedback noise levels. In other words, our approach can be potentially understood as a machine learning-based joint optimization method for feedback coding and error correction coding.


 Figure 9. BLER with $K = 6$ and $N = 18$ for high feedback noise, where the forward SNR is 1dB.

D.2. Short blocklength scenarios

Figure 10a shows BLER with $K = 6$, $N = 21$, and the forward SNR with 1dB. This is the case when Deepcode benefits from the zero padding where a zero bit is added at the end of the bit stream. That is, Deepcode utilize 18 channel uses for transmitting the signals corresponding to $K = 6$ bits, and three channel uses for transmitting the signals corresponding to

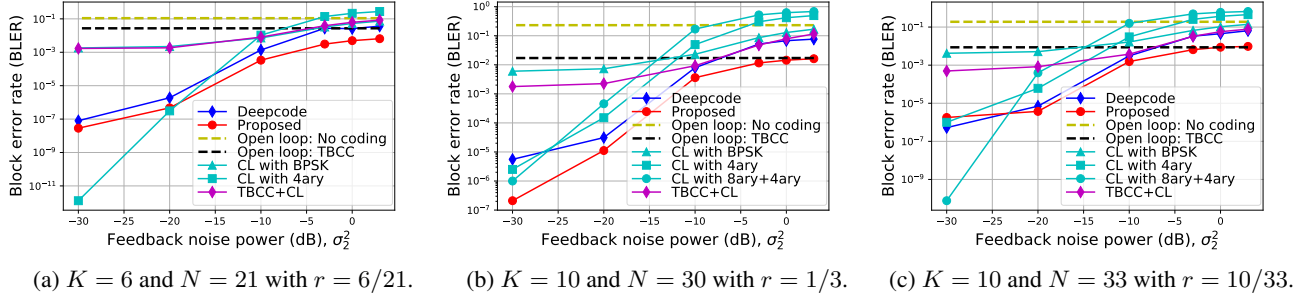


Figure 10. BLER curves with various selections of K and N , where the forward SNR is 1dB.

the padded zero bit. The coding rate is then $r = 2/7$. To be fair, other schemes can use three more channel uses based on $1/3$ -rate coding. Our scheme can generate $2/7$ -rate codes by simply training our RNN autoencoder-based architecture for $K = 6$ and $N = 21$. Although this scenario is favorable for Deepcode, our scheme still outperforms the baselines including Deepcode. Our strategy achieves significant performance gains, as we mentioned in Figure 3, particularly in the regions with strong feedback noise. Figure 10b demonstrates BLER with $K = 10$ and $N = 30$ ($r = 1/3$). In this scenario, our scheme still outperforms the counterparts, and obtain higher performance gains over all the feedback noise regions. Figure 10c shows BLER with $K = 10$ and $N = 33$ ($r = 10/33$), in which Deepcode benefits from using zero padding. Our scheme still performs better than the other baselines in realistic feedback noise power regions as well.

D.3. Medium/long blocklength scenarios

Figure 11 depicts BLER with different blocklength scenarios of $L = 120, 600, 1200$, where the forward SNR is -1 dB and the coding rate is $r = 1/3$. Due to our scheme's tolerance to strong forward noise, it beats existing feedback methods in BLER for any blocklength scenarios by up to two orders of magnitude. For long blocklength scenarios, such as $L = 600, 1200$ in Figure 11b and 11c, any other feedback schemes other than ours cannot outperform canonical turbo coding. However, our scheme outperforms the turbo coding depending on the feedback noise power levels. This demonstrates that, when feedback is available in communication systems, our scheme can be used to improve the BLER performances by exploiting feedback.

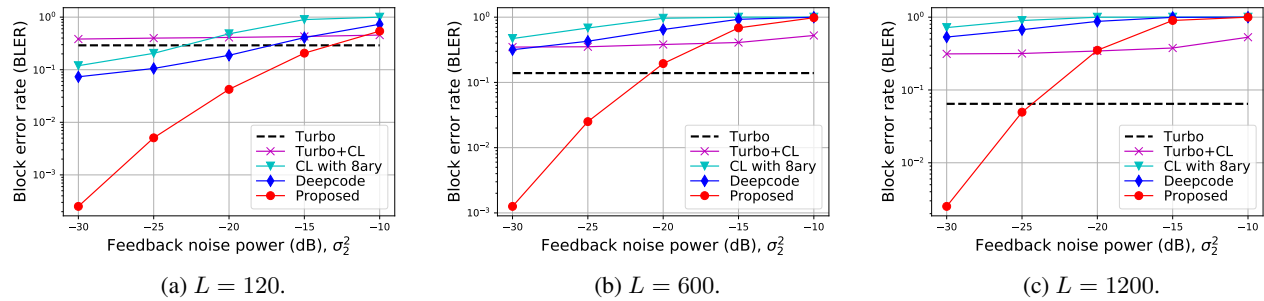


Figure 11. BLER of various selections of blocklength L with $r = 1/3$ when the forward SNR is -1 dB.

E. Power Distribution: Detailed Comparison with CL Scheme

Figure 12 shows power weight distribution along channel uses obtained from using our (non-linear) feedback scheme and the (linear) CL scheme, where the forward SNR is set to 1dB. As discussed in Section 4.4, both linear and non-linear schemes allocate more powers at the start and less powers along timesteps under noisy feedback. Our scheme and the CL scheme, however, exhibit different power distribution patterns along feedback noise levels. For the CL scheme, as the feedback link becomes less noisy, the power distribution becomes even along the channel uses. However, our scheme produces an even power distribution when the feedback noise becomes higher.

The exhibition of different power distribution patterns of our scheme and the CL scheme can be understood by different

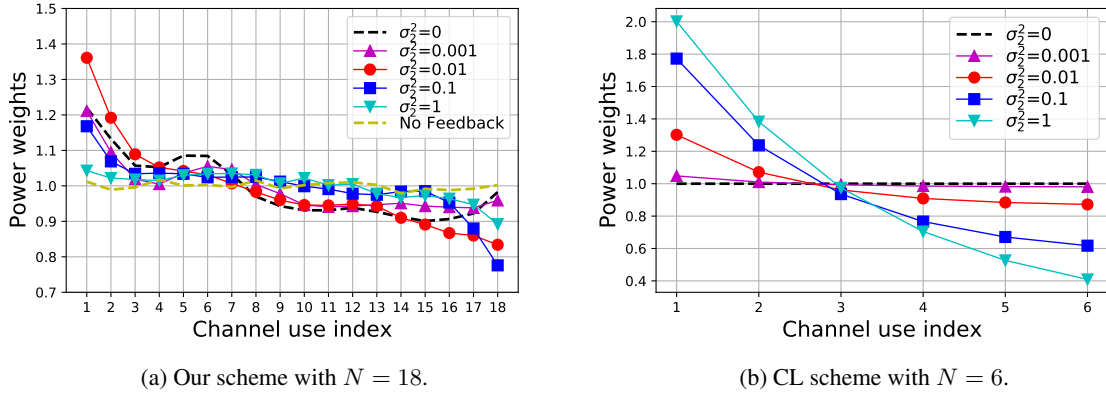


Figure 12. Power distributions over N channel uses obtained by our scheme and the CL scheme.

encoding and decoding processes of the two schemes. First, our scheme has a higher degree of flexibility for feedback coding due to its non-linearity, whereas the feedback codes of the CL scheme are constructed based on the linear assumption. Second, as mentioned in Appendix D.1, our scheme may be regarded to have some combined properties of error correction coding and feedback coding, while the CL scheme is specifically designed for feedback coding. Nevertheless, it is crucial to emphasize that in order to maximize the utilization of the feedback information, both linear and non-linear schemes allocate more powers in the beginning and less powers along channel uses under a noisy feedback scenario with reasonable noise powers.

F. Ablation Studies and Various Configurations for Our Proposed Architecture

F.1. Power control

Table 1 shows the BLER performances obtained from an ablation investigation of our power control scheme, where we consider $K = 6$, $N = 18$, and $r = 1/3$. Since the power control layer consists of the two modules of normalization and power-weight multiplication, we examine the four different cases: (i) both normalization and power-weight multiplication (the default), (ii) just normalization, (iii) just power-weight multiplication, and (iv) neither normalization nor power-weight multiplication. We find that the best results were obtained when both normalization and power-weight multiplication are employed.

Table 1. Ablation study for power control.

	Power/norm	Norm	Power	No power/norm
$\sigma_2^2 = 0.01$	3.34E-6	2.87E-5	4.94E-2	6.29E-2
$\sigma_2^2 = 0.1$	1.63E-3	3.7E-3	5.59E-2	5.52E-2
$\sigma_2^2 = 1$	1.32E-2	1.88E-2	1.26E-1	1.60E-1

F.2. Different number of layers/neurons

Table 2 shows BLER obtained by using our scheme with various numbers of layers and neurons of the GRUs at the encoder and decoder, where we consider $K = 6$, $N = 18$, and $r = 1/3$. We investigate the four examples: (i) a single layer of GRU with 50 neurons, (ii) two layers of GRUs with 50 neurons each (the default), (iii) two layers of GRUs with 100 neurons each, and (iv) three layers of GRUs with 50 neurons each. The encoder and decoder in each scenario will have identical GRU specifications except that the decoder employs bi-directional GRU and the encoder has uni-directional GRU. Overall, we find that case (ii) yields good BLER performances overall. For the scenario with high feedback noise, i.e., $\sigma_2^2 = 0.01$, case (iii) yields the best BLER performance. Given sufficient computational capabilities, we may select the ideal combinations of the number of layers and neurons to obtain the best BLER performances depending on the feedback noise power levels.

Table 2. Study on different number of layers and neurons.

	(1,50)	(2,50)	(2,100)	(3,50)
$\sigma_2^2 = 0.01$	3.16E-6	3.34E-6	1.32E-6	4.48E-6
$\sigma_2^2 = 0.1$	1.85E-3	1.63E-3	1.94E-3	2.19E-3
$\sigma_2^2 = 1$	1.45E-2	1.32E-2	1.40E-2	1.33E-2

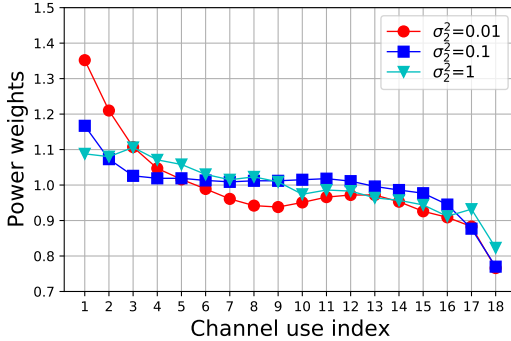
F.3. Uni-directional GRU versus bi-directional GRU at the decoder

Table 3 shows BLER that was obtained by using our scheme either with uni-directional GRU or bi-directional GRU (the default) at the decoder, where we consider $K = 6$, $N = 18$, and $r = 1/3$. In both cases, we consider two layers of GRUs with 50 neurons each at the encoder and decoder. The bi-directional case obtains higher BLERs than those from uni-directional case over the various ranges of feedback powers, despite the uni-directional case yielding comparable performances to the bi-directional case. This is due to the possibility that a non-causal processing of the receive signals could allow the decoder to make better use of the receive signal information.

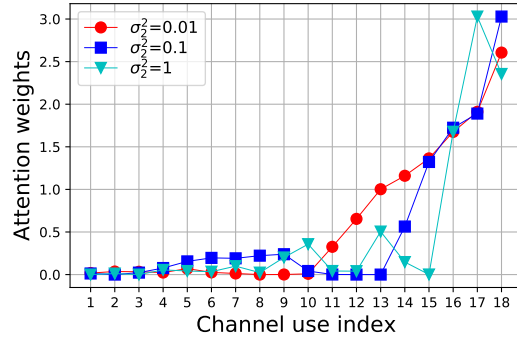
When uni-directional GRU is used in our architecture, we consider the uni-directional attention mechanism with N forward attention weights. Figure 13 shows the distribution of the power weights and the uni-directional attention weights. The power distribution in the uni-directional case in Figure 13a is similar to the one in the bi-directional case. In Figure 13b, the attention weights are higher at the final few channel uses, indicating that the decoder attempts to fully exploit the correlation of all the receive information by focusing on the last few outputs of the forward GRU. As a result, both the uni-directional case and the bi-directional case (in Figure 7) seek to maximally utilize the correlation of the receive signals through optimizing its attention weights.

Table 3. Comparison between uni-directional and bi-directional GRUs at the decoder.

	Uni-directional	Bi-directional
$\sigma_2^2 = 0.01$	5.24E-6	3.34E-6
$\sigma_2^2 = 0.1$	1.73E-3	1.63E-3
$\sigma_2^2 = 1$	1.44E-2	1.31E-2



(a) Power weight distribution



(b) Uni-directional attention weight distribution

Figure 13. The distribution of power weights and attention weights in the case of employing uni-directional GRUs in the proposed RNN autoencoder architecture.

F.4. Different strategies for merging GRU outputs at the decoder

Table 4 shows the BLER performances obtained by using our scheme with various strategies for merging the bi-directional GRU outputs at the decoder, where we consider $K = 6$, $N = 18$, and $r = 1/3$. We explore the following five scenarios: Case 1. We use only the hidden states at the N -th timestep, i.e., $\alpha_{f,N} = \alpha_{b,N} = 1$, while the rest weights are forced to zeros. Case 2. We use the hidden states at the N -th timestep for the forward GRU and at the 1st timestep for the backward GRU, respectively. That is, $\alpha_{f,N} = \alpha_{b,1} = 1$, while the rest weights are zeros. Case 3. We sum the hidden states over all the timesteps equally, i.e., $\alpha_{f,k} = \alpha_{b,k} = 1$ for all $k = 1, \dots, N$. Case 4. We use the attention mechanism to

put different weights along N timesteps, but the same weight is applied for the forward and backward direction at each timestep. That is, $\alpha_k = \alpha_{f,k} = \alpha_{b,k}$ is trainable for all $k = 1, \dots, N$. Case 5. As our default configuration, we use a bi-directional attention mechanism where all separate weights are applied for each timestep as well as for each of the forward and backward directions. That is, we have $2N$ trainable weights, $\alpha_{f,k}$ and $\alpha_{b,k}$, for $k = 1, \dots, N$. We discover that in nearly all of the feedback noise power scenarios, the bi-directional attention mechanism at the decoder produced the best BLER performances.

Table 4. Study on different strategies for merging GRU outputs at the decoder.

	Case 1	Case 2	Case 3	Case 4	Case 5
$\sigma_2^2 = 0.001$	4.37E-7	5.25E-8	2.55E-8	2.31E-8	8.12E-9
$\sigma_2^2 = 0.01$	1.02E-5	4.19E-6	3.78E-6	3.32E-6	3.34E-6
$\sigma_2^2 = 0.1$	2.66E-3	1.97E-3	1.98E-3	1.66E-3	1.63E-3
$\sigma_2^2 = 1$	1.47E-2	1.46E-2	1.38E-2	1.36E-2	1.32E-2

F.5. Sigmoid versus softmax at the last layer at the decoder

Minimizing BLER as a performance metric for bit stream recovery has been the focus of this paper. Other metric of interest is bit error rate (BER). Our architecture can be trained to minimize BER rather than BLER, by simply replacing the softmax activation function with the sigmoid activation function at the decoder and considering the binary cross entropy loss rather than the cross entropy loss. Table 5 and 6 show BLER and BER, respectively, obtained by using our scheme when sigmoid or softmax is applied as an activation function at the last layer at the decoder. We consider $K = 6$, $N = 18$, and $r = 1/3$. In Table 5, using softmax yields better BLER performances as expected since it allows the neural network to be trained while minimizing the block errors. In Table 6, using the sigmoid is not superior to using the softmax in the noise setting $\sigma_2^2 = 0.1$ and 1; rather, its performance is comparable to that of the softmax case. But, at $\sigma_2^2 = 0.01$, utilizing the sigmoid yields a better BER performance. This is because the neural network with the sigmoid function is trained to minimize the bit errors. This demonstrates how our learning architecture can be readily modified to accommodate different metrics of interests.

Table 5. BLER with sigmoid or softmax

	Sigmoid	Softmax
$\sigma_2^2 = 0.01$	3.79E-6	3.34E-6
$\sigma_2^2 = 0.1$	2.61E-3	1.63E-3
$\sigma_2^2 = 1$	3.33E-2	1.31E-2

Table 6. BER with sigmoid or softmax

	Sigmoid	Softmax
$\sigma_2^2 = 0.01$	7.95E-7	1.18E-6
$\sigma_2^2 = 0.1$	5.17E-4	4.60E-4
$\sigma_2^2 = 1$	7.44E-3	6.43E-3